Arabian Journal of Chemistry (2019) **12**, 1413–1423

King Saud University

Arabian Journal of Chemistry

www.ksu.edu.sa
www.sciencedirect.com

ORIGINAL ARTICLE

In situ-preparation and characterization of silver-HEMA/PEGDA hydrogel matrix nanocomposites: Silver inclusion studies into hydrogel matrix

Carmen M. González-Henríquez [a,*], Guadalupe del C. Pizarro [a], Mauricio A. Sarabia-Vallejos [b], Claudio A. Terraza [c], Zoraya E. López-Cabaña [d]

[a] *Chemistry Department, Universidad Tecnológica Metropolitana, J.P. Alessandri 1242, Santiago, Chile*
[b] *Institute of Physics, Pontificia Universidad Católica de Chile, P.O. Box 306, Correo 22, Santiago, Chile*
[c] *Faculty of Chemistry, Pontificia Universidad Católica de Chile, P.O. Box 306, Correo 22, Santiago, Chile*
[d] *Laboratory of Asymmetric Synthesis, Chemistry Institute of Natural Resources, Universidad de Talca, P.O. Box 747, Talca, Chile*

Received 28 July 2014; accepted 3 November 2014
Available online 18 November 2014

KEYWORDS

Silver nanoparticles;
HEMA/PEGDA hydrogel;
Thermal properties;
Crosslinking agent

Abstract Poly(ethylene glycol) diacrylate (PEGDA) of different molecular weights (Mn = 575 and 700) was used as crosslinking agent for the photopolymerization of 2-hydroxyethyl methacrylate (HEMA) in order to obtain HEMA/PEGDA-based hydrogels. Composites were synthesized *in situ* employing a new methodology that implies the addition of different quantities of silver nitrate aqueous solution to the monomer mixture with the finality to obtain hydrogels with different silver nanoparticles' spatial density and distribution. Samples were characterized by thermal, optical, spectroscopic and structural/morphological methods. Thermal studies showed that the increase of PEGDA molecular weight and the $AgNO_3$ concentration in the reaction mixture enhance the glass transition temperature and the thermal stability of the composites. This behavior could be related to the silver coordination with the polymer network. Infrared spectroscopy with Fourier transform and Raman analyses were realized in order to corroborate the sample chemical structure by the identification of specific functional groups. Surface hydrogel morphology was visualized with scanning electron microscopy analysis, detecting a homogeneous micro-porous surface for the samples obtained from high molecular weight PEGDA. Presence of silver nanoparticles was established by X-ray fluorescence spectroscopy and UV/Vis methods. In this last case, the characteristic silver nanoparticle plasmon was observed. Using Transmission Electron Microscopy it was possible to visualize a homogeneous spatial distribution of spherical silver nanoparticles with very narrow

* Corresponding author. Tel.: +56 02 2787 7188.
E-mail address: carmenmabel@gmail.com (C.M. González-Henríquez).

Peer review under responsibility of King Saud University.

Production and hosting by Elsevier

http://dx.doi.org/10.1016/j.arabjc.2014.11.012

diameter distribution that rounds about 14–21 ± 5 nm. In general, the silver nanoparticle presence in the compounds enhances considerably their thermal/morphological characteristics.

1. Introduction

Noble metal nanoparticles have an extremely small size, high specific surface area relative to their volume and a high fraction of surface atoms (Arvizo et al., 2012). These characteristics give them an incredibly high interaction capacity with each other and also with other organic and inorganic structures and make them useful in innumerable biological, biomedical, optical, electronic and quantum size domains applications. Between them it is possible to find uses as catalysts devices (Scholten et al., 2011), semiconductor materials (Tan et al., 2012), solar cells construction, ultrafast data communication and optical data storage (Février et al., 2012), among others (Abou et al., 2010). Production of metal-based nanoparticles by reduction (Wang et al., 2013), thermal treatment (Lopez-Sanchez et al., 2011), irradiation (Sarina et al., 2013) and laser ablation (Fong et al., 2013) oftentimes requires the presence of organic solvents and toxic reducing agents. In this sense, nanomaterials synthesis using organic matrices is an emerging aspect in nanoscience and nanotechnology (Cui et al., 2014). Therefore, biological and biomimetic approaches for nanomaterials synthesis are being explored (Narayanan and Sakthivel, 2010). In accordance with this, a wide variety of polymers have become quite interesting. In particular, hydrogels attract the researchers' attention since their first synthesis due to a perceived "intelligence" and high biocompatibility (Cao et al., 2014). This sort of polymers has been used as thin films, scaffolds and coverings in a wide range of biomedical and biological applications such as tissue engineering (Hoffman, 2012), drug delivery (Panyam and Labhasetwar, 2012), medical diagnostics and therapeutics (Guenther et al., 2013), among others. Polymer networks can be synthesized using various chemical methods, like photo- and thermal-initiated polymerization (Carr et al., 2011; Park and Lee, 2013). This fact allows designing structures with molecular-scale control in order to modulate the material micro-properties such as crosslinking density and molecular weight. So, it is possible to produce improvements in their macro-properties such as biodegradation, mechanical strength, chemical and biological response to stimuli, swelling degree, among others (Barrett et al., 2012).

Neutral synthetic polymers can be generated from derivatives of poly(hydroxyethyl methacrylate) (PHEMA), poly(ethylene glycol) (PEG) and poly(vinyl alcohol) (PVA) (Ren et al., 2013; Tockary et al., 2013). Hydrogels based on PHEMA and PEG are the most widely studied materials and, also, the most used for biomedical applications due to their non-toxicity and non-immunogenic properties, making these types of hydrogels approved by the US Food and Drug Administration for a wide variety of medical uses such as human intravenous injection and oral and dermal applications (Chen et al., 2013). On the other hand, poly(ethylene glycol) diacrylate (PEGDA), used as crosslinking agent, has a high biocompatibility maintaining the PHEMA amphiphilic characteristics. Furthermore, PEGDA can be easily excreted from the body via kidney and liver forming non-toxic metabolites, making them more suitable for tissue engineering and drug delivery applications (Xu et al., 2010).

It is possible to combine inorganic nanoparticles with the hydrogel matrix using a novel method. The process was carried out using PHEMA/PEGDA-based hydrogel photopolymerization (UV radiation exposure) via free radicals in an aqueous solution of $AgNO_3$. The presence of free radicals in the solution trigger the formation and stabilization of silver nanoparticles embedded into the hydrogel network. This conformation improves the nanoparticle biocompatibility and stability.

This research was focused in the formation of silver nanoparticles embedded into the HEMA/PEGDA hydrogel matrix in order to stabilize and protect them of possible oxidation and agglomeration, and also for improving the biocompatibility of the inorganic particles. Our main motivation was focused in the effect that produces the crosslinking agent molecular weight (PEGDA) used in the photo-polymerization process and the amount of silver nanoparticles embedded into the system through the variation of the Ag^+ concentration in the solution using a new and novel synthetic methodology.

Noble-metal nanoparticles formation embedded into the hydrogel matrix were studied by optical measurements such as UV/Vis spectroscopy, Raman spectroscopy, Infrared spectroscopy with Fourier transform (FT-IR), X-ray fluorescence spectroscopy (XRFS) and also via structural measurements such as X-ray diffraction (XRD). In addition, thermal properties were measured by Differential Scanning Calorimetry (DSC) and thermogravimetric analysis (TGA). Size of the metallic nanoparticles was studied by Transmission Electron Microscopy (TEM). Also, scanning electron microscopy (SEM) was employed in order to visualize and measure the polymer surface porosity.

2. Materials and methods

2.1. Chemicals

HEMA (2-hydroxyethyl methacrylate, 97%) containing ⩽250 ppm of monomethyl ether hydroquinone (MEHQ) as inhibitor and PEGDA (poly(ethylene glycol) diacrylate) of Mn = 575 and Mn = 700 containing 400–600 ppm of MEHQ and 300 ppm of butylhydroxytoluene (BHT) as inhibitors; respectively, were used as crosslinking agents. Irgacure 2959 (2-hydroxy-4′-(2-hydroxyethoxy)-2-methylpropiophenone) was used as photo-initiator agent. All the reactants were purchased in Sigma–Aldrich (St. Louis, MO, USA). Ultrapure water for chromatography LiChrosolv was used as dissolvent during the photopolymerization and 1-vinyl-2-pyrrolidone (NVP), stabilized with *N,N′*-di-secbutyl-1,4-phenylenediamine was utilized as dissolvent for the photo-initiator process. Both reagents were acquired from Merck (KGaA, Darmstadt, Germany).

2.2. Equipments and measurements

FT-IR spectra (KBr pellet) were obtained on a Bruker TENSOR 27 (Bruker Optics Inc., Ettlingen, Germany) equipped with a KBr beamsplitter, RockSolid™ interferometer, DigiTect™ detector system and a 1.2 mW, 632.8 nm He–Ne laser. Structural and vibrational properties of the hydrogels and their composites (hydrogel-silver nanoparticles) were characterized by Raman spectroscopy with a LabRam 010 instrument from ISA equipped with a 5.5 mW, 632.8 nm He–Ne laser without filter. Raman microscope uses a back-scattering geometry, where the incident beam is linearly polarized at 500:1 ratio. Microscope objective used to realize the Raman analysis was an Olympus Mplan 50×.

Absorption spectra of the hydrogels pure and their composites were measured in solid state using barium sulfate as standard. These results were recorded at 25 °C between 200 and 800 nm in a UV–Vis spectrophotometer Perkin-Elmer Lambda 35.

Size and morphology of the silver nanoparticles were studied by Transmission Electron Microscopy, using a microscope model Philips Tecnai 12 BioTWIN operated at 120 kV with different magnifications. The grids were brought from Ted Pella, Inc., 300 mesh copper specimen grids with formvar/carbon support films.

Morphology of the composites was examined by conventional scanning electron microscopy (Zeiss/LEO VP1400) via the study of the surface morphology with VPSE (Variable Pressure Secondary Electron) and QBSD (Quadrant Back Scattering) as detectors. Micrographs are obtained by operating the SE microscope at an accelerating voltage of 25 kV.

X-ray fluorescence spectroscopy was realized with a Shimadzu EDX-720 in vacuum through powder sample. Energy dispersion of the X-ray fluorescence was detected with a Si detector with liquid nitrogen for cooling. X-ray was generated with an Rh anode with voltages between 15 and 50 kV and a current of 1 to 1000 μA.

X-ray diffraction analysis were developed at room temperature with a Bruker D-8 Advanced Diffractometer, using a long fine focus ceramic X-ray tube with copper anode (λ(CuKα) = 0.154 nm) working at 2.2 kW. Diffraction patterns were obtained in the usual Bragg–Brentano (θ–2θ) geometry via powder samples in a rotating holder. X-ray tube was operated at 40 kV and 40 mA. Goniometer was swept between 5° and 140° with 0.02° steps in the whole interval. Diffracted X-rays were detected with a NaI dynamic scintillation detector.

DSC traces were recorded on a Mettler Toledo, DSC 822e Differential Scanning Calorimetric from the second heating run. Thermal degradation studies were developed in a TGA/DSC 1 Star e System Mettler Toledo thermobalance. Both analyses were recorded with a heating rate of 20 °C/min under nitrogen atmosphere.

Hydrogels polymerizations were developed through sample radiation exposure using a UV lamp with his emission peak centered at 365 nm (VILBER LOURMAT 230 V, 50/60 Hz, 365 nm, 9 W). Then, in order to eliminate all the occluded water molecules, the samples were subjected to a freeze-dried lyophilization process (Labconco FreeZone 6, 12 L console freeze dry system with purge valve and mini chamber).

2.3. Preparation of HEMA/PEGDA hydrogels containing silver nanoparticles

Preparation of hydrogel was carried out in a glass transparent flask; where 2 g of HEMA (15.368 mmol), 0.089 g of PEGDA-575 (Mn = 575; 0.156 mmol) and 0.0175 g of Irgacure 2959 (0.078 mmol) were dissolved in 50 μL of NVP. Reaction mixture was continuously purged with nitrogen gas in order to displace the air of the system avoiding oxidation processes.

Similar procedure was used to prepare the hydrogel derived from PEGDA-700 (Mn = 700).

Afterward, 1.0, 1.5 and 2.0 mL of $AgNO_3$ aqueous solution (0.5 mol/L) was poured on the reaction mixture, keeping an oxygen-free environment. Then, in dark and an inert atmosphere, the solution was stirred by 30 min until to reach a complete homogenization. Finally, the flask was irradiated at 365 nm with an UV lamp for 30 min; the solution changes its appearance from transparent to light brown color during the photopolymerization process. Once the hydrogels with silver nanoparticles were obtained, the samples were washed with distillated water in order to eliminate the precursor remainders. Finally, the samples were lyophilized for 48 h, and subsequently pulverized in an agate mortar, to obtain a homogeneous powder.

Nanocomposites were designated according with the added volume of Ag^+ to the solution and the molecular weight of PEGDA employed: Ag-Hg2A-1.0, Ag-Hg2A-1.5, Ag-Hg2A-2.0 and Ag-Hg2B-1.0, Ag-Hg2B-1.5, Ag-Hg2B-2.0, where A implies the use of PEGDA-575 and B, PEGDA-700.

3. Results and discussion

3.1. Hydrogels and HEMA/PEGDA hydrogels-nanoparticles systems

Procedure used to obtain silver nanoparticles into a hydrogel matrix and initiate polymerization include the free radicals formation produced in the photo-initiation, which attaches the vinyl group of the monomer and the same time originate the reduction of Ag^+ to metallic silver. This fact explains the change observed in the appearance of the system during the photopolymerization process, which implies to pass of transparency to a light brown color. So, the synthesized nanoparticles were embedded into the polymeric matrix, which promotes a certain protection to the metal.

Formation mechanism of silver nanoparticles involves two parallel processes: photoreduction (direct photolysis) and photosensitization (Scheme 1). Both process were produced at the same time when the reaction mixture (monomers + solution of $AgNO_3$ + Irgacure 2959) was exposed to UV irradiation. Thus, the Ag° particles were formed by direct $AgNO_3$ photoreduction and also, metallic reduction using photochemically generated intermediates. Formation of free radicals were produced by the homolytic cleave of Irgacure 2959, reducing the metal ions to generate nanoparticles (Sakamoto et al., 2009). These same radicals also attach to the vinyl group of HEMA/PEGDA producing polymerization.

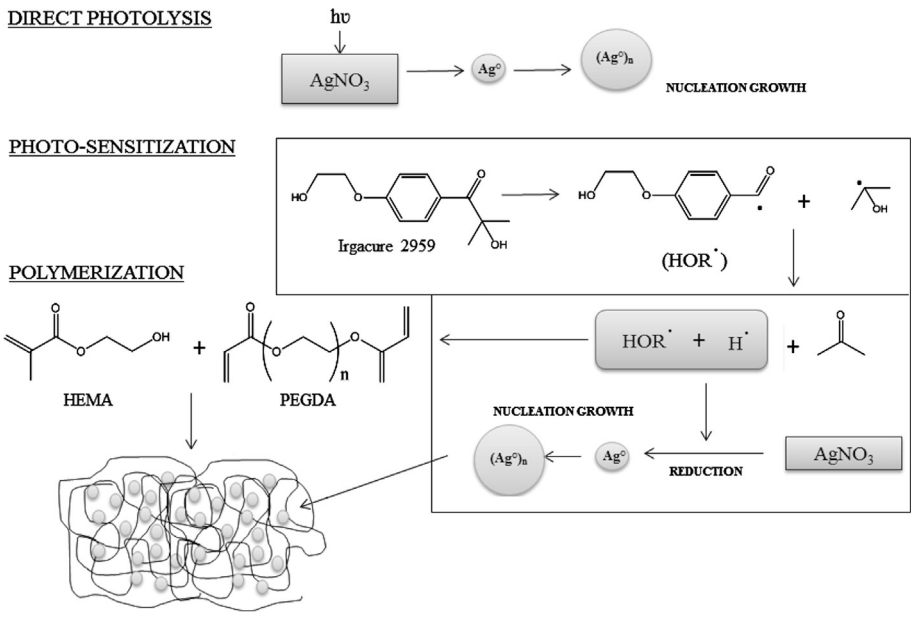

Scheme 1 Reaction mechanism proposed to obtain the silver nanoparticles/hydrogel matrix systems.

3.2. FT-IR and Raman spectra analyses

Spectroscopic studies were realized in order to corroborate the chemical structure of the hydrogels, via the identification of specific functional groups. In addition, with these techniques, also it is possible to verify the effect of the nanoparticle formation over the hydrogel matrix and the crystallinity of the system. Fig. 1 shows the FT-IR and Raman spectra for the hydrogel based on PEGDA-700 and two nanocomposites samples obtained from the same Ag^+ concentration and different PEGDA.

3.2.1. HEMA/PEGDA-700 hydrogel (Hg2B)

FT-IR (KBr, *v*, cm^{-1}): 3435 (stretching, —OH (free), *vb*); 2984–2880 (stretching, CH_3, CH_2, CH and three bands OH (H-bonded), *s*); 1725 (stretching, C═O ester, *m*); 1453 (bending, CH_2 and CH_3 deformation, *m*); 1390 (bending, CH_3 deformation and OH bending (in-plane, *ip*), *m*); 1159 (stretching, C—O—OR ester, *s*); 1059 (stretching C—OH, *m*); 743 (bending, CH_2 rocking and OH bending (out-of-plane, *oop*), *m*). **Raman** (*v*, cm^{-1}): 3483 (stretching, intermolecular polymeric OH hydrogen bonded, *s*); 3006–2886 (stretching, CH_3 (antisym.) and CH_2 (sym.) vibration – three bands, *vs*); 1727 (stretching, unconjugated C═O, *m*); 1454 (bending, CH_3 vibration, antisym. and CH_2 scissoring, *s*); 1324 (bending, involving —C—O ester bond, *w*); 1271–1205, 1124–1086 (stretching, C—C skelt., *s-m*); 1028 (stretching, *oop* C—C—OH, *m*); 962 (stretching C—O—R, *m*); 897–820 (stretching, C—C skelt. and *ip* C—C—OH, *s-m*); 608 (bending, O—C═O *ip* deformation, *m*).

3.2.2. Ag-Hg2A-2.0 nanocomposite

FT-IR (KBr, *v*, cm^{-1}): 3448 (stretching, —OH (free) and sym. H_2O, *b*); 2982–2917 (stretching, CH_3, CH_2, CH and three bands, OH (H-bonded) and antisym. H_2O, *w*); 1720 (stretching, C═O ester, *m*); 1641 (bending, H_2O, *m*); 1465 (bending, CH_2 and CH_3 deformation, *w*); 1276 (bending, CH_3 deformation and OH bending (*ip*), *w*); 1159 (stretching, C—O—OR ester, *w*); 1078 (stretching C—OH, *w*). **Raman** (*v*, cm^{-1}): 3481 (stretching, intermolecular polymeric OH hydrogen bonded and liquid H_2O, *s*); 3001–2882 (stretching, CH_3 (antisym.) and CH_2 (sym.) vibration – three bands, *vs*); 1727 (stretching, unconjugated C═O, *w*); 1629 (bending, liquid H_2O, *w* (Lin-Vien et al., 1991); 1456 (bending, CH_3 vibration, antisym., and CH_2 scissoring, *s*); 1274–1233 and 1125–1084 (stretching, C—C skelt., *w*); 1024 (stretching, *oop* C—C—OH, *m*); 966 (stretching C—O—R, *w*); 600 (bending, O—C═O *ip* deformation, *m*).

3.2.3. Ag-Hg2B-2.0 nanocomposite

FT-IR (KBr, *v*, cm^{-1}): 3452 (stretching, —OH (free) and sym. H_2O, *b*); 2992–2873 (stretching, CH_3, CH_2, CH and three bands, OH (H-bonded) and antisym. H_2O, *w*); 1717 (stretching, C═O ester, *m*); 1647 (bending, H_2O, *m*); 1461 (bending, CH_2 and CH_3 deformation, *w*); 1262 (bending, CH_3 deformation and OH bending (*ip*), *w*); 1165 (stretching, C—O—OR ester, *w*); 1081 (stretching C—OH, *w*). **Raman** (*v*, cm^{-1}): 3473 (stretching, intermolecular polymeric OH hydrogen bonded and liquid H_2O, *s*); 2992–2890 (stretching, CH_3 (antisym.) and CH_2 (sym.) vibration – three bands, *vs*); 1721 (stretching, unconjugated C═O, *w*); 1651 (bending, liquid H_2O, *w*); 1454 (bending, CH_3 vibration, antisym., and CH_2 scissoring, *s*); 1271–1233 and 1116–1085 (stretching, C—C skelt., *w*); 1025 (stretching, *oop* C—C—OH, *m*); 962 (stretching C—O—R, *w*); 597 (bending, O—C═O *ip* deformation, *m*).

According with the results (Fig. 1b and c), the nanocomposites contain liquid H_2O, evidenced by specific signals. This behavior could be associated to the amount of nanoparticles distributed in the system, producing a finite number of defects in where the water should be occluded. This effect is accompanied by possible interaction of water with the surface remaining silver, which could explain the observed modes for O—H stretching and O—H *in-plane* bending.

Raman spectra show that although the pure hydrogel is amorphous, just as it is evidenced in the X-ray analysis (Fig. 5), it is more crystalline than the composites that present

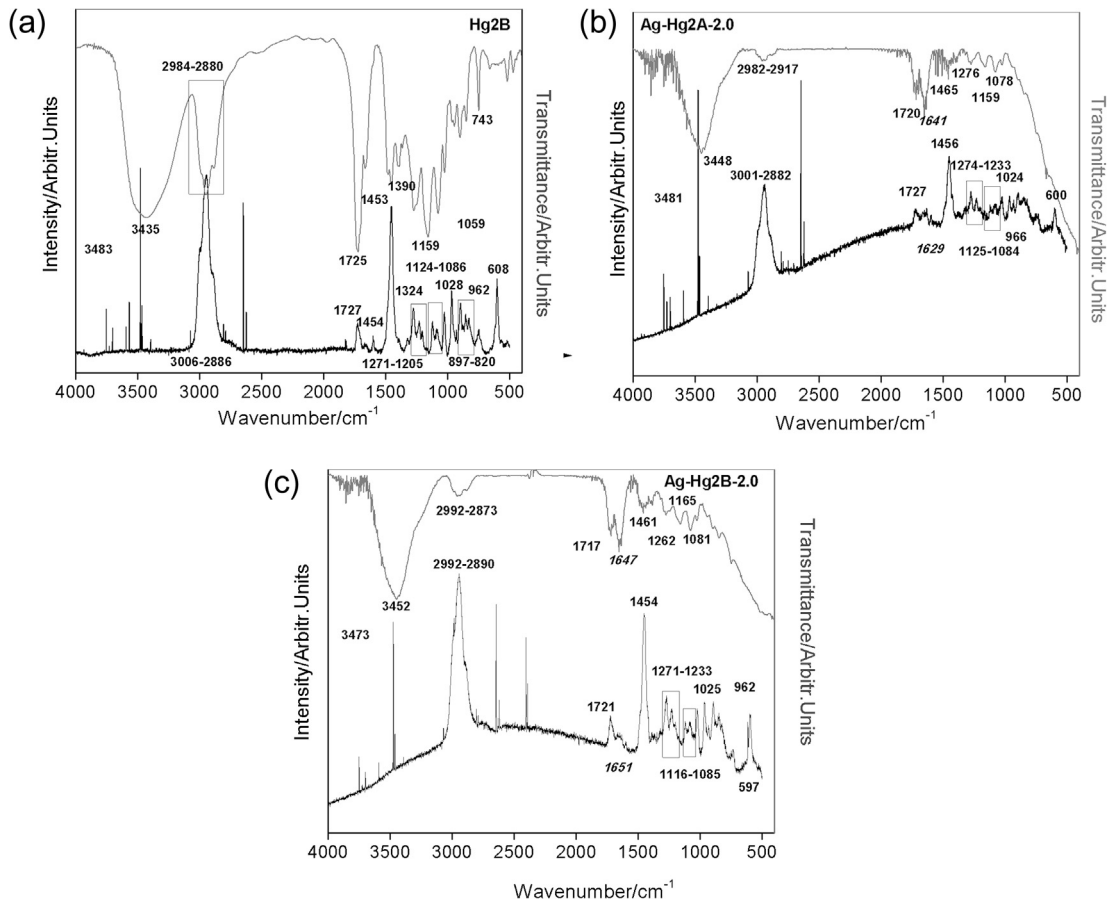

Figure 1 FT-IR/Raman spectra of: (a) HEMA/PEGDA-700 hydrogel pure (Hg2B), (b) Ag-Hg2A-2.0 nanocomposite and (c) Ag-Hg2B-2.0 nanocomposite.

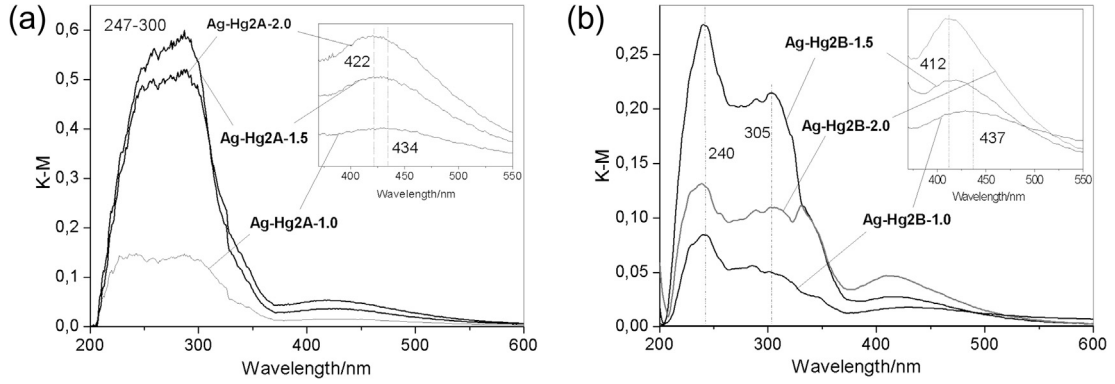

Figure 2 UV/Vis diffuses reflectance spectra for (a) Ag-Hg2A and (b) Ag-Hg2B.

silver nanoparticles embedded into the polymeric matrix. Thus, the metallic particles inclusion increases the steric hindrance between the polymeric chains, producing a packing disorder and therefore an increment in the system amorphicity, represented by a low intensity and definition of the bands.

3.3. Optical properties

Presence of silver nanoparticles into of the hydrogel matrix was established using diffuse-reflectance UV/Vis spectroscopy. In Fig. 2a and b is possible to identify the characteristic surface plasmon resonance of silver nanoparticles that appears at 422–434 nm and 412–437 nm for Ag-Hg2A and Ag-Hg2B; respectively. This last nanocomposite has a higher band intensity compared with Ag-Hg2A. Additionally, these composites present an electronic transition of metallic silver that appears in the ~250–330 nm spectral range (Lu et al., 2005). This ensemble of bands is overlapped with the π–π^* and n–π^* transition corresponding to the C═O group of the HEMA and PEGDA.

Surface plasmon absorption related to the silver nanoparticles into the hydrogel matrix is affected by the Ag^+ concentration used in the synthesis. Thus, a blue shift was observed

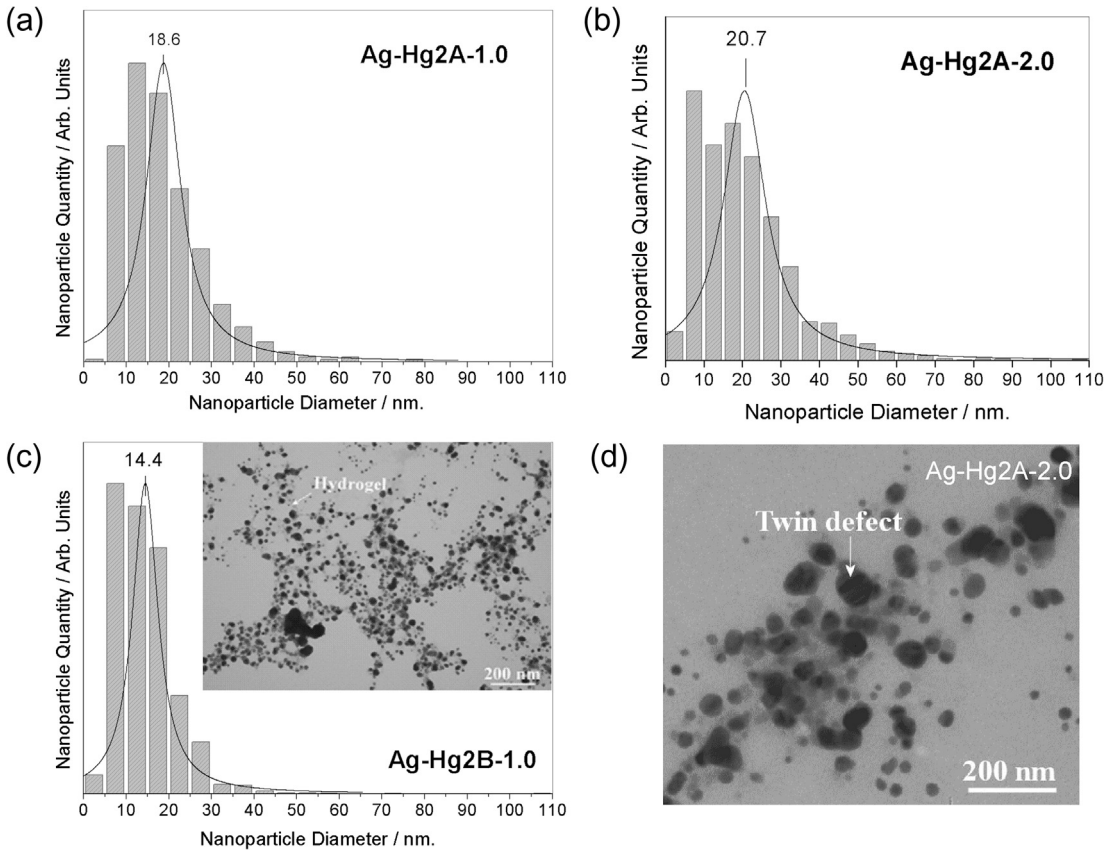

Figure 3 Histograms of: (a) Ag-Hg2A-1.0; (b) Ag-Hg2A-2.0; (c) Ag-Hg2B-1.0 inset a representative image at 60000x and (d) TEM image of a twin defect in silver nanoparticles (Ag-Hg2A-2.0 composite).

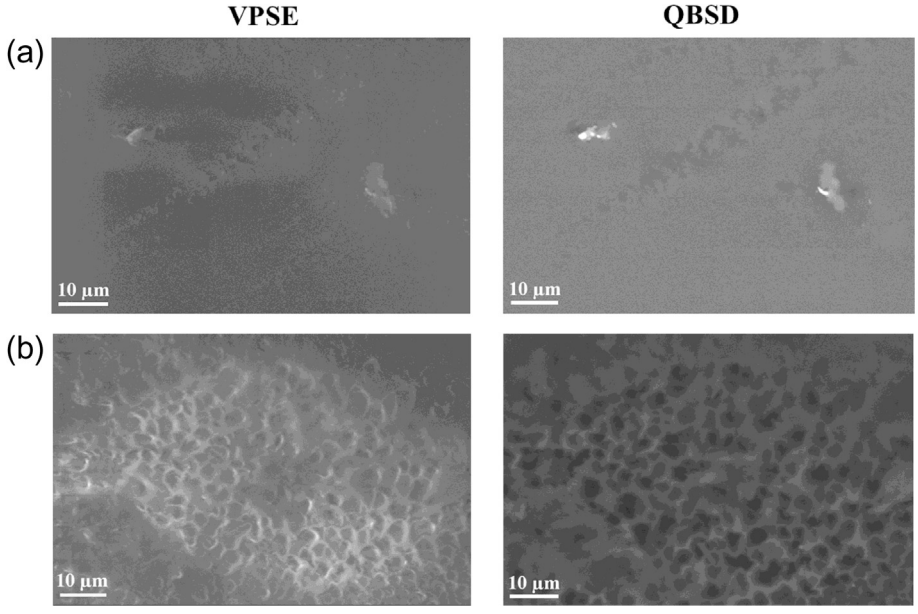

Figure 4 SEM images using two kinds of detectors: VPSE and QBSD for (a) Ag-Hg2A-2.0 and (b) Ag-Hg2B-2.0 composites.

when the concentration of $AgNO_3$ decreased. Therefore, the variation in the peak width and its position suggest that the size of the silver nanoparticles will be altered if the Ag^+ ion concentration is changed, producing possibly agglomeration of silver nano-crystals into the system (Cook et al., 2011). Decrease of $AgNO_3$ concentration produces a wavelength increase, due to the decrease of the nanoparticle size into hydrogel matrix. This behavior was corroborated by TEM.

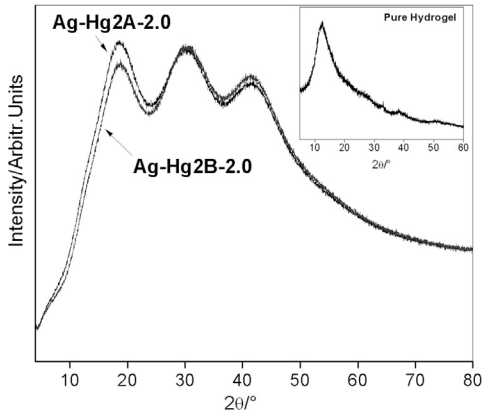

Figure 5 X-ray diffraction for the nanocomposites and the pure hydrogel.

Shape difference of silver surface plasmon between samples with the same crosslinking agent molecular weight is neatly related to the collective oscillation of electrons when it is stimulated with light. Thus, the silver nanoparticles create a dipolar oscillation in the compounds surface. When the frequency of the electromagnetic fields becomes resonant with the coherent electron motion, a strong absorption takes place. This absorption depends on the particles size (cluster formation) and also, on the environment that surrounds to the metal. For this motive, the composites that present higher $AgNO_3$ concentrations also have a band most prominent displaced to wavelength minor.

3.4. Morphological studies

3.4.1. Transmission Electron Microscopy

Silver nanoparticle size, embedded in HEMA/PEGDA-based hydrogel matrix, was determined by TEM measures. Fig. 3c and d illustrates the micrographs obtained and the histograms respective are shown in Fig. 3a–c. From these figures, the diameter and the distribution size of the silver nanoparticles for Ag-Hg2A-1.0, Ag-Hg2A-2.0 and Ag-Hg2B-1.0 composites, respectively are calculated.

Histograms compare the nanoparticle diameters with their quantity. Lorentzian curves were fitted to the distributions; the curve center corresponds to the average nanoparticle diameter. For the samples Ag-Hg2A-1.0 (Fig. 3a) and Ag-Hg2A-2.0 (Fig. 3b) the average silver nanoparticle size is 18.6 ± 4.7 nm and 20.7 ± 5.7 nm, respectively. These results allow to conclude that the increment in the $AgNO_3$ solution concentration in the reaction mixture increases the diameter of silver nanoparticle into hydrogel matrix. This behavior fits with the obtained in diffuse reflectance analyses (Fig. 2) in the sense that the silver nanoparticle size is proportional to Ag^+ ion concentration in the initial reaction mixture.

In Ag-Hg2B-1.0 composite obtained from PEGDA-700, the average diameter of silver nanoparticles in the hydrogel matrix is 14.4 ± 4.8 nm (Fig. 3c). On the other hand, when the average diameter of the nanoparticles obtained for the same Ag^+ concentration (Ag-Hg2A-1.0 with 18.6 nm and Ag-Hg2B-1.0 with 14.4 nm) is compared, it is possible to observe that the molecular weight of the crosslinking agent (PEGDA) do not affect significantly the silver nanoparticle size formed into hydrogel matrix.

Micrograph obtained for Ag-Hg2B-1.0 (inset in Fig. 3c) shows that the silver nanoparticles have spherical shape (dark area) with a very homogeneous spatial and size distribution. Also, it is possible to visualize gray fibers (dark gray area) that connect the nanoparticles between them. This bunch structure corresponds to the hydrogel matrix that encapsulates and protects the silver nanoparticles.

During the exploration of the sample in the microscope, it is possible to observe that the silver nanoparticles might collapse probably due to the high temperature generated by the electron beam. Fig. 3d shows a twin defect on silver nanoparticles (Langille et al., 2012); effect commonly observed in metallic crystalline structures. In this case, two separate crystals share their lattice points symmetrically, like a mirror. These defects form a twin boundary that is possible to visualize as light and dark lines interspersed.

3.4.2. Scanning electron microscopy

Surface morphology of the composites was studied by SEM using VPSE and QBS as detectors and the results are shown in Fig. 4a and b.

Images of Ag-Hg2A-2.0, nanocomposite derived from PEGDA-575 (Fig. 4a), shows a more homogenous surface than those observed for the sample Ag-Hg2B-2.0 (Fig. 4b). Thus, the nanocomposite formed with the crosslinking agent of highest molecular weight (PEGDA-700) presents large numbers of interconnected pores producing the formation of porous structure, which are clearly showed by QBSD detector as a contrast change. It is important to note that the spherical shapes observed on the surface in Fig. 4b are not attributed to silver metal nanoparticles. In accordance with Mengjun et al. (2013), the metal has a tendency to agglomerate due to high surface energy and surface tension of the ultrafine nanoparticles.

Energy dispersive spectroscopy (EDS) results show absence of silver to level surface, probably due to the nanoparticles small size and to the high encapsulation degree of the polymer matrix around of them. Thus, this technique only showed the presence of C: 64.20%, O: 35.40%, Al: 0.54% and C: 65.55%; O: 32.18% and Al: 2.27% for Ag-Hg2A-2.0, and Ag-Hg2B-2.0 nanocomposite, respectively. Small amount of aluminum could be related to the impurities produced by the material used in the composite preparation.

3.4.3. X-ray fluorescence spectroscopy

Amount of silver nanoparticles embedded into the polymer matrix (Ag-Hg2A-2.0 and Ag-Hg2B-2.0) was detected via the measure of pressed pellets by XRFS technique. Both compounds indicate a 100% presence of silver element into the system. It is important to highlight that this technique only can detect elements with AMU over 22, which means that elements like C, O or H cannot be detected with this technique; therefore the organic part of the hydrogel could not be studied with this methodology.

3.4.4. X-ray diffraction

Fig. 5 shows XRD patterns for the nanocomposites Ag-Hg2A-2.0 and Ag-Hg2B-2.0. Both composites do not present diffraction peaks at 2θ = 38.3° (111), 44.4° (200), 64.6° (220), 77.5° (311) and 81.7° (222), signals that are attributed to pure metallic silver (a = 4.086 Å, JCPDS file No. 04-0783). These

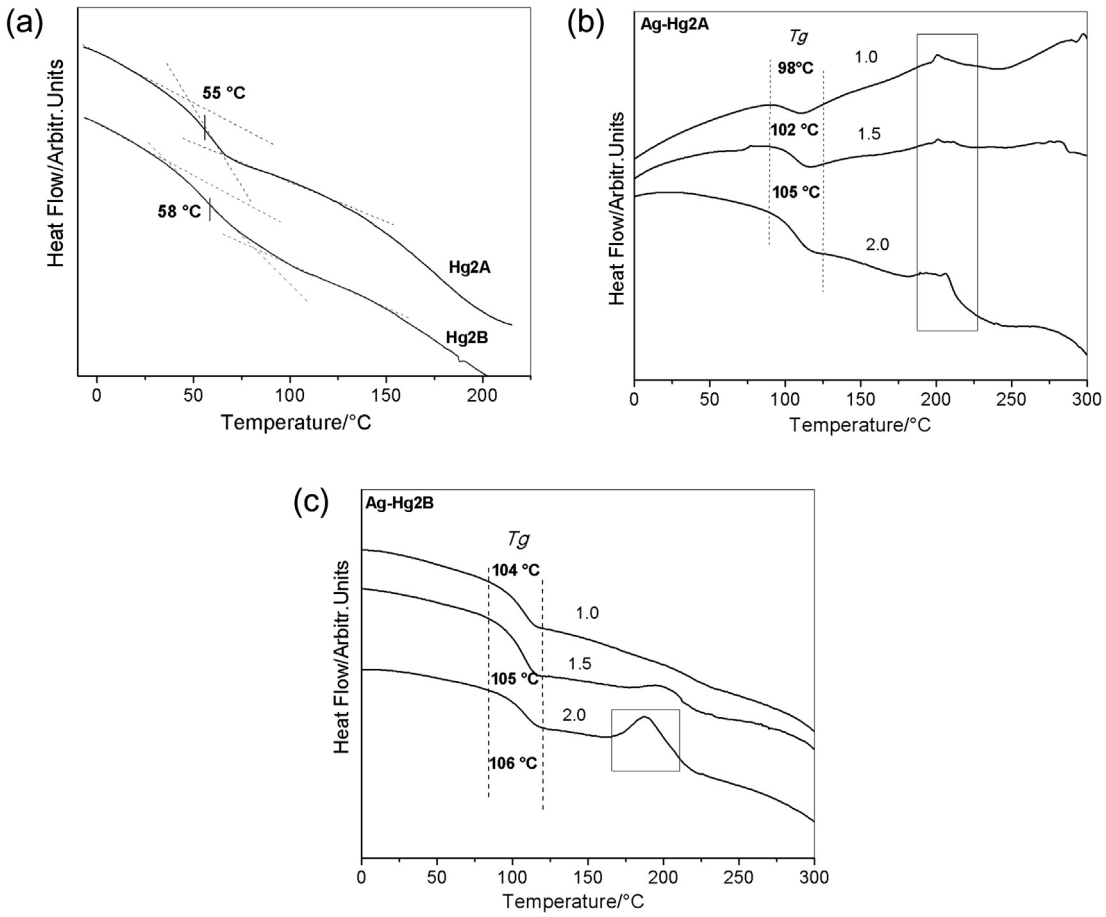

Figure 6 DSC traces by: (a) Hg2A and Hg2B; (b) Ag-Hg2A at different volumes of $AgNO_3$ solution (0.5 mol/L) and (c) Ag-Hg2B at different volumes of $AgNO_3$ solution (0.5 mol/L).

data confirm that the high amorphicity of the compound prevents the visualization of the diffraction peaks attributed to the nanoparticles, where the polymer encapsulation around silver nanoparticles also helps the non-detection of XRD diffraction peaks.

Amorphicity of a pure hydrogel is shown in the top right image of Fig. 5. Both samples (Hg2A and Hg2B) present similar diffraction pattern, associated to the irregularity of their polymeric chains and to the crosslinking degree (packing degree); characteristics transmitted to the nanocomposites. This same effect was showed by Raman analyses (Fig. 1b and c). On the other hand, at the same Ag^+ concentration, the molecular weight of the crosslinking agent did not affect the shape or intensity of the diffraction pattern observed form the nanocomposites.

3.5. Thermal properties

3.5.1. Differential scanning calorimetry

DSC curves of pure hydrogels and their composites are shown in Fig. 6. Mixture between silver nanoparticles and the polymeric matrix obtained from PEGDA-575 and PEGDA-700 exhibited a single glass transition temperature (*Tg*). This fact is associated to the miscibility blends obtained; probably implicating intra- e inter-molecular interactions that favor the stability of the resulting system.

Pure hydrogels (Fig. 6a) show an only *Tg* at 55 °C (Hg2A) and in 58 °C (Hg2B), respectively, attributed to the material originated from the mixture between HEMA (Yao et al., 2010) and PEGDA of different molecular weights. Crosslinking agent confers a diminution in the *Tg* of HEMA (atactic configuration: 85–100 °C, (Wypych, 2011)), forming a new compound with properties totally different to the precursors used in the polymerization (Xu et al., 2010). Additionally, the temperature difference between these two systems (3 °C) is related to the cross-linking agent molecular weight.

PEGDA-700 originates a polymeric network slightly more rigid in comparison to those obtained from PEGDA-575. Fig. 6b shows a slight increase in the *Tg* of the materials from 98 °C to 105 °C when the Ag^+ concentration is increased. This result could be explained due to a loss of flexibility of the polymeric chains when the metallic nanoparticles are associated with them. These interactions induce a partial crystallization that is observed near to 200 °C and it is most notorious for the sample that contains the highest Ag+ concentration (Ag-Hg2A-2.0). Similar tendency is showed for the nanocomposites obtained from PEGDA-700 (Ag-Hg2B; Fig. 6c).

3.5.2. Thermogravimetric analysis

These studies were carried out in order to evaluate the thermal stability and degradation profile of the pure hydrogels and their nanocomposites. The results are summarized in Fig. 7

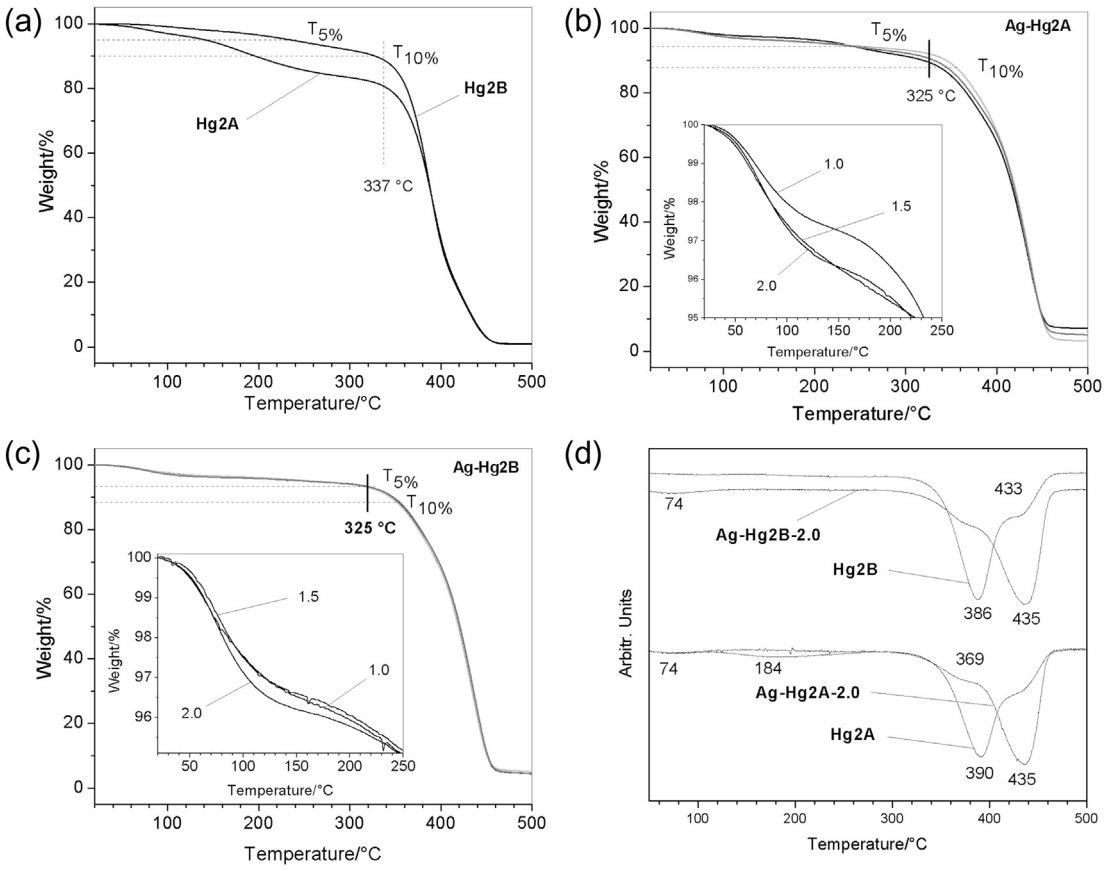

Figure 7 Thermogravimetric analysis: (a) Hg2A and Hg2B; (b) Ag-Hg2A at different volumes of $AgNO_3$ solution (0.5 mol/L); (c) Ag-Hg2B at different volumes of $AgNO_3$ solution (0.5 mol/L) and (d) derivatives traces for hydrogels and theirs composite obtained for the same Ag^+ concentration.

Table 1 Thermal degradation profiles of the hydrogels and their silver nanocomposites.

System	[a]$T_{5\%}$	[b]$T_{10\%}$	[c]Char yield
Hg2A	**142**	**195**	**0.8**
Ag-Hg2A-1.0	233	320	7.2
Ag-Hg2A-1.5	224	345	3.2
Ag-Hg2A-2.0	221	332	5.1
Hg2B	**236**	**327**	**1.0**
Ag-Hg2B-1.0	251	347	4.5
Ag-Hg2B-1.5	258	345	5.1
Ag-Hg2B-2.0	251	348	4.5

The vaules in bold represent the thermal properties of the original polymers, without nanoparticles.
[a,b] Temperatures at which 5% and 10% weight loss was recorded by TGA at a heating rate 20 °C/min in N_2 atmosphere, respectively.
[c] Percentage weight at 500 °C.

and Table 1. In addition, the amounts of nanoparticles are shown in Table 2.

Hydrogel Hg2A shows three steps in its thermal degradation process (Fig. 7a). The first step occurs between 58 °C and 138 °C, accompanied with the weight loss of 1% and 5%, respectively. This first degradation process could be assigned to the residual loss water used in the synthesis and in cleaning methods. Following loss weight is observed between 140 °C and 330 °C approximately and it should correspond to the thermal decomposition of the PHEMA matrix.

Table 2 Nanoparticle content into hydrogel at 490 °C.

System	Nanoparticle amount (Ag°)		
	1.0[a]	1.5[a]	2.0[a]
Hg2A	6.4% (0.34 mg)	2.4% (0.17 mg)	4.4% (0.32 mg)
Hg2B	3.6% (0.28 mg)	4.2% (0.30 mg)	3.7% (0.30 mg)

Amount of sample added to crucible (TGA): Ag-Hg2A-1.0 (5.4 mg); Ag-Hg2A-1.5 (7.2 mg) and Ag-Hg2A-2.0 (7.3 mg)/Ag-Hg2B-1.0 (7.7 mg); Ag-Hg2B-1.5 (7.2 mg) and Ag-Hg2B-2.0 (8.2 mg).
[a] Volume (mL) of $AgNO_3$ aqueous solution (0.5 mol/L).

Finally, the PEGDA matrix is decomposed with temperatures starting at 337 °C. This fast and clean process finished at 460 °C approximately, almost without organic residues (< 1% in both samples). This last step in the degradation profile is most notorious in the sample Hg2B (Fig. 7a). Thus, the difference observed in the thermal degradation process is related neatly with the chain size of the crosslinking agent employed in the synthesis of the hydrogel matrix. Therefore, when the molecular weight of PEGDA is increased from 575 (A) to 700 (B), its thermal stability also increase, due to the high degree of network crosslinking.

Fig. 7b and c shows a first mass loss near to 80 °C associated probably to the volatilization of the residual water. The inclusion of silver nanoparticles affects the thermal degradation of the system, due to the interaction between them and the organic matrix. This fact is easily observable in Fig. 7d which shows the derivative traces for pure hydrogels and their composites. Main thermal event that affect to the samples is displaced at higher temperatures (40 °C approximately) when silver is incorporated to the polymeric matrixes. Incorporation of the same concentration of Ag^+ do not affect significantly the degradation process of the samples, maintaining a similar profile and thermal decomposition temperature (435 °C).

Table 1 shows the temperatures at which 5% and 10% weight was loss, respectively. It is clear that the $AgNO_3$ concentration used in the synthesis of the nanocomposites affects the thermal stability of them. Thus, although their starting decomposition temperature is slightly lower compared to the pure hydrogels; the composite present higher decomposition temperature.

At 490 °C is possible to detect 0.8% and 1.0% of residual charge for Hg2A and Hg2B, respectively (Fig. 7a), leading to almost complete mass loss for these compounds. At this temperature only is possible to find inorganic structures (silver nanoparticles). Using these different amounts of residual charge between hydrogel (control) and hydrogel/silver nanoparticle systems is possible to obtain the content of nanoparticles into the polymer, leaving in evidence the following results: 6.4% (Ag-Hg2A-1.0), 2.4% (Ag-Hg2A-1.5) and 4.4% (Ag-Hg2A-2.0) of metal structures (Table 2). These differences could be related to thermal stability given by silver nanoparticles to the system (Fig. 7b). According to this hypothesis, the thermal stability of Ag-Hg2B is similar between the samples that have different volumes of $AgNO_3$ solution: 3.6% (Ag-Hg2B-1.0), 2.4% (Ag-Hg2B-1.5) and 4.4% (Ag-Hg2B-2.0).

It is important to mention that the volume (1.0, 1.5 or 2 mL of $AgNO_{3(aq)}$/0.5 M) placed in the reaction mixture before polymerization is different to the amount of silver nanoparticles embedded into the polymer matrix, due to the effect of the crosslinking degree (PEGDA-575 and 700) which favors the formation of some microdomains with irregular concentration of silver nanoparticles into the system.

4. Conclusions

Pure hydrogels studied by Raman and FT-IR spectroscopy show more define bands than their respective composite (nanoparticles embedded into the polymer), implying that the metal nanoparticles produce a structural packing disorder in the polymer chains. Silver surface plasmon was detected by diffuse-reflectance UV/Vis spectroscopy, ensuring the presence of silver nanoparticles in the system. Thus, the most pronounced band is related to the composite synthesized with highest crosslinking agent molecular weight and with the highest concentration of $AgNO_3$. Furthermore, the silver nanoparticles into the hydrogel produce a higher glass transition temperature and a partial crystallization, according to the results obtained by DSC technique. In addition, the composite thermal stability increase could be related to silver coordination polymer network. Amorphicity of hydrogel and the encapsulation of the polymer around the nanoparticles prevent the detection of silver bands in the XRD spectra, being this a useless technique to identify the nanoparticles into of the hydrogel matrix. SEM micrographs indicate that some nanoparticles could agglomerate and form porous surfaces with the crosslink agent increase in the solution mixture. TEM studies permit to conclude that the shape-, spatial- and size-distribution of the nanoparticles into hydrogel matrix are very homogeneous.

According to this, it was demonstrated that the *in situ* synthesis of the composites via photopolymerization constitute a new way to form homogeneous silver nanocomposites with thermal stability.

Acknowledgments

Authors acknowledge the financial support of this work by FONDECYT Grant N° 11121281 and 1110836. C.M. González-Henríquez acknowledges to the attraction and insertion of Advanced Human Capital Program, PAI 7912010031-CONICYT. M. Sarabia-Vallejos acknowledges the financial support given by CONICYT through the Magister Scholarship Grant.

References

Abou, K.M.M., Eftaiha, A., Al-Warthan, A., Ammar, R.A.A., 2010. Synthesis and applications of silver nanoparticles. Arab. J. Chem. 3, 135–140.

Arvizo, R.R., Bhattacharyya, S., Kudgus, R.A., Giri, K., Bhattacharya, R., Mukherjee, P., 2012. Intrinsic therapeutic applications of noble metal nanoparticles: past, present and future. Chem. Soc. Rev. 4, 2943–2970.

Barrett, D.G., Fullenkamp, D.E., He, L., Holten-Andersen, N., Lee, K.Y.C., Messersmith, P.B., 2012. pH-based regulation of hydrogel mechanical properties through mussel-inspired chemistry and processing. Adv. Funct. Mater. 23, 1111–1119.

Cao, Y., Mei, M.L., Li, Q.L., Lo, E.C.M., Chu, C.H., 2014. Agarose hydrogel biomimetic mineralization model for the regeneration of enamel prism like tissue. ACS Appl. Mater. Interfaces 6, 410–420.

Carr, L.R., Zhou, Y.B., Krause, J.E., Xue, H., Jiang, S.Y., 2011. Uniform zwitterionic polymer hydrogels with a nonfouling and functionalizable crosslinker using photopolymerization. Biomaterials 32, 6893–6899.

Chen, W., Zheng, M., Meng, F., Cheng, R., Deng, C., Feijen, J., Zhong, Z., 2013. In situ forming reduction-sensitive degradable nanogels for facile loading and triggered intracellular release of proteins. Biomacromolecules 14, 1214–1222.

Cook, W.D., Nghiem, Q.D., Chen, Q., Chen, F., Sangermano, M., 2011. Simultaneous photoinduced silver nanoparticles formation and cationic polymerization of divinyl ethers. Macromolecules 44, 4065–4071.

Cui, Q.H., Zhao, Y.S., Yao, J., 2014. Tailoring the structures and compositions of one-dimensional organic nanomaterials towards chemical sensing applications. Chem. Sci. 5, 52–57.

Février, M., Gogol, P., Aassime, A., Mégy, R., Delacour, C., Chelnokov, A., Apuzzo, A., Blaize, S., Lourtioz, J.M., Dagens, B., 2012. Giant coupling effect between metal nanoparticle chain and optical waveguide. Nano Lett. 12, 1032–1037.

Fong, Y.Y., Gascooke, J.R., Visser, B.R., Harris, H.H., Cowie, B.C.C., Thomsen, L., Metha, G.F., Buntine, M.A., 2013. Influence of cationic surfactants on the formation and surface oxidation states of gold nanoparticles produced via laser ablation. Langmuir 29, 12452–12462.

Guenther, M., Gerlach, G., Wallmersperger, T., Avula, M.N., Cho, S.H., Xie, X., Armstrong, T., 2013. Smart hydrogel-based biochemical microsensor array for medical diagnostics. Adv. Sci. Technol. 85, 47–52.

Hoffman, A.S., 2012. Hydrogels for biomedical applications. Adv. Drug Deliv. Rev. 64, 18–23.

Langille, M.R., Zhang, J., Personick, M.L., Li, S., Mirkin, C.A., 2012. Stepwise evolution of spherical seeds into 20-fold twinned icosahedra. Science 337, 954–957.

Lin-Vien, D., Colthup, N.B., Fateley, W.G., Grasselli, J.G., 1991. The Handbook of Infrared and Raman Characteristic Frequencies of Organic Molecules. Academic Press, San Diego, New York, Boston, London, Sydney, Tokyo, Toronto.

Lopez-Sanchez, J.A., Dimitratos, N., Hammond, C., Brett, G.L., Kesavan, L., White, S., Hutchings, G.J., 2011. Facile removal of stabilizer-ligands from supported gold nanoparticles. Nat. Chem. 3, 551–556.

Lu, J., Bravo-Suárez, J.J., Takahashi, A., Haruta, M., Oyama, S.T., 2005. In situ UV–Vis studies of the effect of particle size on the epoxidation of ethylene and propylene on supported silver catalysts with molecular oxygen. J. Catal. 232, 85–95.

Mengjun, C., Yining, Z., Wantai, Y., Meizhen, Y., 2013. UV-irradiation-induced templated/in-situ formation of ultrafine silver/polymer hybrid nanoparticles as antibacterial. Langmuir 29, 16018–16024.

Narayanan, K.B., Sakthivel, N., 2010. Biological synthesis of metal nanoparticles by microbes. Adv. Colloid. Interface Sci. 156, 1–13.

Panyam, J., Labhasetwar, V., 2012. Biodegradable nanoparticles for drug and gene delivery to cells and tissue. Adv. Drug Deliv. Rev. 64, 61–71.

Park, C.H., Lee, J., 2013. pH-dependent sustained release characteristics of disulfide polymers prepared by simple thermal polymerization. J. Biomater. Sci. Polym. Ed. 24, 1848–1857.

Ren, T., Mao, Z., Guo, J., Gao, C., 2013. Directional migration of vascular smooth muscle cells guided by a molecule weight gradient of poly(2-hydroxyethyl methacrylate) brushes. Langmuir 29, 6386–6395.

Sakamoto, M., Fujistuka, M., Majima, T., 2009. Light as a construction tool of metal nanoparticles: synthesis and mechanism. J. Photochem. Photobiol. C: Photochem. Rev. 10, 33–56.

Sarina, S., Zhu, H., Jaatinen, E., Xiao, Q., Liu, H., Jia, J., Chen, C., Zhao, J., 2013. Enhancing catalytic performance of palladium in gold and palladium alloy nanoparticles for organic synthesis reactions through visible light irradiation at ambient temperatures. J. Am. Chem. Soc. 135, 5793–5801.

Scholten, J.D., Leal, B.C., Dupont, J., 2011. Transition metal nanoparticle catalysis in ionic liquids. ACS Catal. 2, 184–200.

Tan, H., Santbergen, R., Smets, A.H.M., Zeman, M., 2012. Plasmonic light trapping in thin-film silicon solar cells with improved self-assembled silver nanoparticles. Nano Lett. 12, 4070–4076.

Tockary, T.A., Osada, K., Chen, Q., Machitani, K., Dirisala, A., Uchida, S., Nomoto, T., Toh, K., Matsumoto, Y., Itaka, K., Nitta, K., Nagayama, K., Kataoka, K., 2013. Tethered PEG crowdedness determining shape and blood circulation profile of polyplex micelle gene carriers. Macromolecules 46, 6585–6592.

Wang, X., Altmann, L., Stöver, J., Zielasek, V., Bäumer, M., Al-Shamery, K., Borchert, H., Parisi, J., Kolny-Olesiak, J., 2013. Pt/Sn intermetallic, core/shell and alloy nanoparticles. Colloidal synthesis and structural control. Chem. Mater. 25, 1400–1407.

Wypych, G., 2011. Handbook of Polymers. ChemTec Publishing, Ontario, Canada.

Xu, L.Q., Yao, F., Fu, G.D., Kang, E.T., 2010. Interpenetrating network hydrogels via simultaneous "click chemistry" and atom transfer radical polymerization. Biomacromolecules 11, 1810–1817.

Yao, F., Xu, L., Fu, G.D., Lin, B.P., 2010. Sliding-graft interpenetrating polymer networks from simultaneous click chemistry and atom transfer radical polymerization. Macromolecules 43, 9761–9770.